Monte Carlo simulation of solvent effects on vibrational and electronic spectra[a)]

Michael F. Herman[b)]

Department of Chemistry, Tulane University, New Orleans, Louisiana 70118

Bruce J. Berne

Department of Chemistry, Columbia University, New York, New York 10027
(Received 22 July 1982; accepted 11 August 1982)

Solvent effects on vibrational states are treated in the Born–Oppenheimer approximation. A Monte Carlo procedure is devised for simulating a system in which the vibrations are treated as quantum degrees of freedom and all other degrees of freedom are treated classically. The key to this method is the use of a restructured perturbation theory for solving the vibrational Schrödinger equation at each of the solvent configurations sampled. This method also is used to compute Franck–Condon factors. The methods developed are applied to two different problems. First, solvent effects on vibrational transitions in the ground electronic state are considered. It is found that the frequency shift from the gas phase frequency is to the red at low solvent densities, but to blue at high solvent densities. Secondly, the heterogeneous electronic absorption and emission line shapes are simulated in a variety of model solute–solvent systems and the results are discussed in terms of a simple theoretical model.

I. INTRODUCTION

Monte Carlo[1] and molecular dynamics[2] techniques are valuable tools for the calculation of equilibrium and nonequilibrium statistical mechanical and thermodynamic quantities for classical systems. Currently, Monte Carlo procedures are being developed for semiclassical[3,4] and quantum mechanical systems[5–8] as well. However, there are many systems of chemical interest for which classical mechanics provides an accurate description of the motion of nearly all the degrees of freedom, except for a small number (possibly only one) of coordinates that require a quantum mechanical description.[9] Application of a fully quantum method to these problems would be an inefficient route to take.

In this paper, we consider a simple system of this type: a diatomic molecule in a monatomic solvent. The vibrational motion is not classical at ordinary temperatures. On the other hand, classical mechanics is certainly adequate for the analysis of the translational degrees of freedom. Furthermore, it is assumed throughout that the moment of inertia of the diatomic is sufficiently large so that the classical description of the rotational motion is valid. This classical rotation approximation will break down at low and moderate temperatures for diatomics which contain H, and possibly D, due to their low moments of inertia. Thus, these diatomics are excluded from consideration in this work, although the possible extension to include quantum rotations is discussed briefly in Sec. IV.

Because little is known about the true intermolecular potential energy, we adopt the following model here. The intramolecular potential of the solute is taken to be the RKR potential[10] for the isolated molecule corresponding to the electronic state of interest. The diatomic is assumed to consist of two sites, and the solvent molecules are each assumed to consist of several sites (one if they are monatomic). Each site on the diatomic interacts through a central potential with each site on every solvent molecule. Thus, we invoke a site–site model. In addition, the sites on different solvent molecules interact with each other. To model electrostatic interaction, charges (and polarizabilities, etc.) can be ascribed to sites and the Coulomb terms can be summed. In general, the potential parameters for the solute site–solvent site interactions and the charges on the diatomic sites will be different for different electronic states of the solute. These parameters are also expected to depend on the instantaneous bond length of the diatomic molecule. The choice of electronic state dependent parameters allows us to study solvent effects on electronic absorption and emission spectra.

Starting with the Schrödinger equation for all the degrees of freedom, the Born–Oppenheimer approximation[11] is made, effectively separating the "fast" vibrational motion from the "slow" rotations and translations. The classical limit[9,12] is applied to the quantum mechanical canonical density matrix in such a way that the vibrational factor remain quantum mechanical while the rotational and translational parts go over to their respective classical forms, thus yielding a mixed quantum-classical density matrix. The distribution function is a product of a classical $\exp(-\beta V)$ factor and a quantum-vibrational distribution function, which depends parametrically on the value of the coordinates for the slow motions, as would be expected intuitively. This mixed quantum-classical distribution function can be employed as a sampling function for the ordinary Metropolis Monte Carlo procedure.[13]

This formulation requires the determination of the vibrational energies and corresponding eigenfunctions

[a)]Supported by grants from the National Science Foundation (NSF CHE 81-10284) and the National Institutes of Health NIH GM 26588-06).

[b)]This work was initiated while M. F. Herman was a Research Associate at Columbia University.

 0021-9606/83/064103-15$2.10

for every sampled solvent configuration. This is the time consuming part of the simulation. We show how this can be done efficiently by using a reorganized perturbation theory that is shown to be rapidly convergent for the determination of the states, energies, and Franck–Condon factors for the low lying vibrational states. In a subsequent paper we extend this approach using wave packet dynamics.

The adiabatic approximation is considered in Sec. II A and the procedure for application of the mixed quantum-classical Monte Carlo and molecular dynamics simulation is presented. The perturbative method for the solution of the vibrational Schrödinger equation with the solvent-dependent potential is presented in detail in Sec. II B. A method for simulating electronic absorption and emission spectra is outlined in Sec. II C.

The results of Monte Carlo simulations for a model of Br_2 dissolved in Ar are discussed in Sec. III A for various densities. The observed density dependent shifts in the average vibrational frequency and the nonsymmetric shapes of the frequency distributions are particularly interesting. The average frequency decreases at moderate densities (relative to the gas phase frequency), while at higher densities it increases. This behavior is very reminiscent of the density dependence of the frequency shift that is experimentally observed in many systems.[14] The interaction potential employed includes a specific model for the bond length dependence of the Ar–Br_2 interaction.[9] It has been suggested[15,16] that this bond length dependence has important effects on the equilibrium properties of the oscillator, and we find that the red shift in the average frequency at moderate densities is essentially absent if this aspect of the potential is not included in the model. The density dependence of the peak position and shape of the frequency distributions are analyzed in terms of a simplified model in Sec. III A. In Sec. III B methods developed in Sec. II are used to simulate the electronic absorption and emission spectra of a model diatomic for several different solvent–solute potentials. The observed solvent induced shifts are readily understood on the basis of simple arguments. Finally, in Sec. IV the major results of this work are summarized and possible extensions of these approaches are discussed.

II. THEORY

A. Adiabatic approximation for an oscillator in a solvent

In this section, we treat systems consisting of one diatomic molecule in a dense monatomic fluid. The time scale for vibrational motion is, in most cases, orders of magnitude faster than the other motions present. These other slow motions include rotation and translation of the diatomic, and translation of the solvent particles. This separation of time scales suggests a Born–Oppenheimer approximation.

Let r be the vibrational coordinate (bond length) and let the set $\{\mathbf{X}\}$ represent all the slow coordinates. The Hamiltonian for our systems is

$$H = T_S + T_f + V(r,\{\mathbf{X}\}) = T_S + H_f \tag{2.1}$$

where T_S and T_f are kinetic energy operators for the slow and fast variables, respectively. The wave function for the entire system can be approximated as

$$\Psi(r|\mathbf{X}) = \psi(r|\mathbf{X})\,\Phi(\mathbf{X}) , \tag{2.2}$$

where $\psi(r|\mathbf{X})$ is an eigenfunction of H_f, the Hamiltonian for the fast degree of freedom at fixed $\{\mathbf{X}\}$, i.e.,

$$H_f\psi(r|\mathbf{X}) = E_f(\chi)\psi(r|\mathbf{X}) . \tag{2.3}$$

The adiabatic approximation consists of substitution of Eqs. (2.2) and (2.3) into Eq. (2.1) and ignoring the terms involving derivatives of $\psi(r|\mathbf{X})$ with respect to the slow variables. This approximation yields the following equation for the slow variables:

$$\{T_S + E_f(\mathbf{X})\}\,\Phi(\mathbf{X}) = E_T\Phi(\mathbf{X}) , \tag{2.4}$$

where E_T is the total energy of the full system. The vibrational energy levels, $E_f(\mathbf{X})$, calculated for fixed $\{\mathbf{X}\}$, act as the potential energy surfaces which governs the evolution of the slow variables.

As is usually the case, we assume that the spacings of energy levels corresponding to the slow degrees of freedom is much smaller than $k_B T$. If this is the case, then classical mechanics provides an accurate description for these motions. Thus, the rotational and translational motions evolve classically according to Hamilton's equation of motion,[17]

$$\dot{\mathbf{X}}_S = \partial H_S/\partial \mathbf{P}_S , \qquad \dot{\mathbf{P}}_S = -\partial H_S/\partial \mathbf{X}_S , \tag{2.5}$$

where the Hamiltonian for the slow degrees of freedom is

$$H_S = T_S + E_f(\mathbf{X}) \tag{2.6}$$

and $\{\mathbf{P}_S\}$ is the set of generalized momenta conjugate to the positions $\{\mathbf{X}\}$,

$$P_{Si} = \partial T_S/\partial \dot{X}_i . \tag{2.7}$$

Note that the potential surface $E_f(\mathbf{X})$ also depends on the quantum state of the oscillator, and the trajectory of the slow variables will differ for different vibrational levels.

This stiuation is, of course, exactly analogous to the usual Born–Oppenheimer separation of the electronic and nuclear motions. Adiabatic electronic energy surfaces are obtained for fixed nuclear configurations. The nuclear motions take place on these surfaces. The classical limit corresponds to running classical trajectories for the nuclear degrees of freedom on a given electronic surface.

For many purposes, only thermally averaged quantities are desired, as opposed to dynamical information about the evolution of the system subject to specific initial conditions. In this case, the quantity of interest is the canonical density matrix. In an earlier publica-

tion,[9] we have shown that, after the classical limit has been taken for the slow variables, the density matrix in the position representation is,

$$\rho(r, r'; \beta | \mathbf{X}) = A(\beta) \sum_n \psi_n^*(r | \mathbf{X}) \psi_n(r' | \mathbf{X}) e^{-\beta E_n(\mathbf{X})} . \quad (2.8)$$

In Eq. (2.8), ψ_n and E_n are the wave function and energy for the nth vibrational state at the fixed values of the rotational and translational coordinates, $\{\mathbf{X}\}$, $\beta = (k_B T)^{-1}$, k_B is the Boltzmann constant, T is the temperature, and $A(\beta)$ is a temperature dependent constant arising from the integrations over the momenta $\{\mathbf{P}_S\}$, conjugate to the slow variables. For the particular case of a diatomic in a monatomic fluid,

$$A(\beta) = (2\pi M k_B T/h^2)^{3N/2} (2\pi m k_B T/h)^{3/2} (2\pi I k_B T/h^2), \quad (2.9)$$

where N is the number of solvent particles and h is Planck's constant. M, m, and I are, respectively, the mass of a solvent particle, the reduced mass of the diatomic, and the moment of inertia of the diatomic, respectively. In order to facilitate the integrations over the momenta conjugate to the diatomic rotational angles θ and ϕ, the term $L^2/2mr^2$ in T_S has been replaced with $L^2/2I$, where $I = mr_e^2$ and r_e is the equilibrium bond length for the isolated diatomic.

A number of ensemble averaged quantities are of interest. For example, the average bond length is given by

$$\langle r \rangle = Z^{-1} \int d\mathbf{X}\, dr\, r \rho(r, r; \beta | \mathbf{X}) . \quad (2.10)$$

The average total energy of the system is given by

$$\langle E \rangle = \left\{ \frac{3N+5}{2} \right\} k_B T + Z^{-1} \int d\mathbf{X}\, dr \{ H_f \rho(r, r'; \beta |) \}_{r=r'} . \quad (2.11)$$

The term $\{(3N+5)/2\}\, k_B T$ is the average kinetic energy T_S, in the classical limit. It contains contributions of $3Nk_BT/2$, and $3k_BT/2$ and k_BT, from the translations of the solvent particles, the translations of the diatomic center of mass and the rotations of the diatomic, respectively. The second term on the right in Eq. (2.11) can obviously be rewritten as $Z^{-1} \int d\mathbf{X} \sum_n E_n(\mathbf{X}) \times \exp[-\beta E_n(\mathbf{X})]$.

For some purposes, it may be desirable to average over an ensemble which corresponds to a diatomic in one particular vibrational state, while the translations and rotations are distributed according to an equilibrium canonical distribution. In this case, the appropriate constrained density matrix to be averaged over is

$$\rho_n(r, r'; \beta | \mathbf{X}) = A(\beta) \psi_n(r | \mathbf{X}) \psi_n(r' | \mathbf{X}) e^{-\beta E_n(\mathbf{X})} . \quad (2.12)$$

It is possible to study ensemble average properties in systems such as those we have been discussing by using the standard Metropolis Monte Carlo sampling procedure[13] to generate a set of points which are distributed, in the limit of a large sample, according to $Z^{-1}\rho(r, r; \beta | \mathbf{X})$ or $Z_n^{-1}\rho_n(r, r; \beta | \mathbf{X})$, [where $Z_n = \int d\mathbf{X}\, dr\, \rho_n(r, r; \beta | \mathbf{X})$]. It is also possible to determine the distribution function of the solvent atoms around a solute molecule in a given vibrational state, irrespective of its bond length by sampling from

$$P_n(\mathbf{X}) = \int dr \rho_n(r, r; \beta | \mathbf{X}) \quad (2.13)$$

[or from $P(\mathbf{X})$, obtained by replacing ρ_n by ρ in Eq. (2.13)].

Since the details of the particular sampling procedure that we employ are straightforward and have been presented elsewhere,[9] we do not restate them here. The point that is worth emphasizing again, however, is that this method required solving the adiabatic (fixed configuration) vibrational Schrödinger equation (2.3) a large number of times. Thus, it is imperative that the method of solution of this differential equation be organized so that it is as efficient as possible for the problem at hand. The method that we employ is described in detail in Sec. II B. Given that such a fast and accurate procedure is available, the method that has been discussed in the present section allows for the realistic, detailed study of the effects of a classical solvent on the quantum vibrational motion of the diatomic.

The procedure outlined in Sec. II B for solving the vibrational Schrödinger equation can also yield the derivatives of the vibrational state energies with respect to the slow variables. These are needed to calculate the forces required to run trajectories in the phase space of the translation and rotations, according to Eq. (2.6). Therefore, molecular dynamics calculations for the mixed quantum-classical systems are also feasible. Since the vibrational degree of freedom is treated quantum mechanically, the time step chosen for the classical trajectory need reflect only the time scales of the motions of the slow variables, and not the (possibly much shorter) time scale appropriate for the vibrational motion.

B. Solution of the vibrational Schrodinger equation

In this section we examine the perturbative solution procedure of the Morse oscillator where

$$V_M(r) = D_e\{1 - \exp[-\alpha(r - r_e)]\}^2 \quad (2.13)$$

is a prototype for the general vibrational potential. The reference Hamiltonian is the harmonic oscillator Hamiltonian where the harmonic frequency ω is chosen to be

$$\omega = [2D_e \alpha^2/m]^{1/2} , \quad (2.14)$$

m is the reduced mass of the oscillator. With this choice for ω, the second derivatives of $V_M(r)$ and the harmonic oscillator potential $V_{HO}(r) = m\omega^2(r - r_e)^2/2$ agree at r_e.

Expanding the perturbation in a power series we have

$$V_M(r) - V_{HO}(r) = \hbar\omega \sum_{n=3}^{\infty} d_n y^n , \quad (2.15)$$

where the dimensionless length is defined as $y = (m\omega/\hbar)^{1/2}(r - r_e)$, and d_n is given by

$$d_n = \frac{1}{n!\,\hbar\omega}\left(\frac{\hbar}{m\omega}\right)^{n/2}\left(\frac{d^n V_M}{dr^n}\right)_{r_e} . \tag{2.16}$$

The derivatives are evaluated at r_e. Noting that the nth derivative of V_M is proportional to $D_e\,\alpha^n$, it is a simple task to show that d_n is of order λ^{n-2} where $\lambda = (\hbar\omega/D_e)^{1/2}$. For typical chemical bonds, λ is a small quantity and Eq. (2.16) provides us with a small expansion parameter for developing a perturbation theory. This expansion in λ is easily obtained by rearranging the familiar Rayleigh Schrödinger perturbation theory (RSPT) expansion.

Computationally useful expressions are obtained by dividing the reference Hamiltonian and the perturbation by $\hbar\omega$. The state energies are simply calculated by multiplying the scaled perturbation expansion by $\hbar\omega$. The scaled reference Hamiltonian is simply

$$H_R = -\tfrac{1}{2}(d^2/dy^2) + \tfrac{1}{2}y^2 . \tag{2.17}$$

The zeroth order energies of the Morse oscillator are given by $(n+1/2)\hbar\omega$. The first order (in λ) contributions to the energies are

$$E_n^{(1)} = d_3\langle n|\,y^3\,|n\rangle\,\hbar\omega \tag{2.18}$$

which vanish due to symmetry.

The second order corrections are

$$E_n^{(2)} = \left[d_4\langle n|\,y^4\,|n\rangle + d_3^2\sum_{k\neq n}\frac{|\langle n|\,y^3\,|k\rangle|^2}{(n-k)}\right]\hbar\omega . \tag{2.19}$$

The first term in the brackets in Eq. (2.19) comes from first order RSPT, while the other term comes from second order RSPT. The matrix elements $\langle n|\,y^p\,|k\rangle$ are evaluated using the states of the reference Hamiltonian H_R. The denominator $(n-k)$ is merely the difference of zeroth order energies of H_R.

If the expressions for d_3, d_4, and the matrix elements $\langle n|\,y^4\,|n\rangle$ and $\langle n|\,y^3\,|k\rangle$ are inserted into Eq. (2.19) (recall $\langle n|\,y^3\,|m\rangle \neq 0$ only if $n = m\pm 1,\ \pm 3$) we find (after a little work)

$$E_n^{(0)} + E_n^{(2)} = (n+1/2)\,\hbar\omega - (n+1/2)^2(\hbar\omega/4D_e)\,\hbar\omega \tag{2.20}$$

which is the exact result for the Morse oscillator energies.[18] Therefore, all higher order terms in λ must be identically zero. For instance, the fourth order term in λ has many contributions which are individually nonzero but which can be shown to exactly cancel. One of these terms arises in first order in ordinary RSPT, another in second order, another in third, and the remaining terms in fourth order. By arranging the perturbation expansion in orders of λ we take advantage of this cancellation. For the general anharmonic oscillator, there is not an exact cancellation. Nevertheless, the cancellation should be considerable if in Eqs. (2.15) and (2.16) d_n is evaluated by replacing V_M with the real potential V and the derivatives are evaluated at the potential minimum.

Sprandel and Kern[19] have numerically studied the convergence of various perturbation expansions for anharmonic oscillator systems. Their work provides evidence of the superior convergence of a perturbation expansion which treats the cubic term in the Taylor series of the perturbation potential [Eq. (2.15)] as order one, the quartic term as order two, etc. We feel that the analysis of the Morse oscillator presented here provides added insight into this problem.

Every term in the energy expansion can be separated into two factors, one which depends on the solvent configuration and one which does not. The configuration dependent factors are products of $\hbar\omega$ and a number of d_n's. These depend on the derivatives of the total potential evaluated at the equilibrium bond length. The remaining factors consist of products of matrix elements of the scaled reference Hamiltonian $\langle n|\,y^m\,|k\rangle$ divided by scaled energy differences $(n-k)$. These may involve summations of the states of H_R. Since these factors only depend on H_R, they remain constant as the solvent configuration changes. Therefore, they need to be evaluated once in the course of a simulation. The computational advantage arises from the fact that these configuration independent factors contain the time consuming portion of the perturbation calculation, the matrix elements and sums over states. A similar analysis applies to the expansion for the wave functions.

Fourth order perturbation theory (in λ) is employed in the Monte Carlo simulations discussed in the next section. At each step in the calculation the minimum of the total potential must be located with respect to bond length. Defining $r_m(\mathbf{X})$ to be this configuration dependent equilibrium bond length, $V(r_m, \mathbf{X})$ and the first six derivatives of V with respect to r must be evaluated at $r_m(\mathbf{X})$ in order to obtain the needed d_n. The perturbation expansion for the state energies measured relative to the potential minimum $V(r_m, \mathbf{X})$ are then evaluated as just described. In molecular dynamics simulations or in force biased Monte Carlo simulations the forces are needed. This involves differentiation with respect to solvent coordinates of $V(r_m, \mathbf{X})$ and the perturbation expansion for the vibrational energy levels.

Care must be taken to correctly account for the fact that r_m also changes as $\mathbf{X}$ varies. Thus the total rate of change of some quantity A with respect to X_i is given by

$$\frac{\partial A}{\partial X_i} = \left(\frac{\partial A}{\partial X_i}\right)_{r_m} + \left(\frac{\partial A}{\partial r}\right)_{X_i}\left(\frac{\partial r_m}{\partial X_i}\right) , \tag{2.21}$$

where X_i and r are treated as independent variables on the right-hand side of Eq. (2.21). $\partial r_m/\partial X_i$ is obtained from the condition that $[\partial V(r, X)/\partial r]_{r_m} = 0$ which follows from the definition of r_m. Thus, the total rate of change of $\partial V/\partial r$ with respect to variations in X_i must vanish. When inserted into Eq. (2.21) this gives the condition

$$0 = \frac{\partial^2 V}{\partial X_i\,\partial r} + \frac{\partial^2 V}{\partial r^2}\,\frac{\partial r_m}{\partial X_i} , \tag{2.22}$$

where the derivatives of V are evaluated at r_m. Eq. (2.22) can be solved for $\partial r_m/\partial X_i$.

C. Electronic spectra

Consider two electronic states of a diatomic molecule labeled A and B, where state A is the ground state and state B is some excited state. In the isolated molecule,

the nuclear potentials for these states are given by RKR potential curves. Given the potential models described in the introduction, each configuration of the solvent produces two new potential curves. Because the solvent is being treated classically, the modulation of these curves is adiabatic and no transitions are induced by solvent fluctuations, only the curves and the associated vibrational states and energies are changed. For each solvent configuration, we can use the methods developed in Sec. II B to compute the low-lying vibrational states and energies for the two potentials and thereby the transition energies. To compute the strength of the transition, we must be able to compute the accompanying Franck–Condon factors—a problem we return to shortly. For each solvent configuration, we thus obtain the transition energies and Franck–Condon factors. If we sample the initial solvent configuration using our Monte Carlo algorithm (Sec. II A) with the molecule being in the ground electronic state, we have all the information required to compute the electronic absorption spectrum within the scope of the model. On the other hand, if the solvent configurations are sampled with the molecule initially in the excited electronic state, the resulting spectrum is the fluorescence spectrum. In time resolved fluorescence, the molecule is excited by a pulse of light on a time scale short compared to the relaxation times of the fluid, but because emission takes place on a nanosecond time scale, the fluoresence spectrum taken at intervals of time after excitation will show an evolution from a spectrum consistent with solvent configurations in equilibrium with the ground electronic state of the molecule to a spectrum consistent with the fluid being in equilibrium with the excited electronic state of the molecule. The present study gives both the initial and final fluorescence spectra, but not the time evolution of the spectra. The time evolution can, nevertheless, be simulated. This is accomplished by sampling initial solvent configurations with the molecule in its ground state. Each of these configurations provides an initial state for a molecular dynamics simulation where the forces are computed using the excited state potential surface. The time evolution of the solvent then generates the new configurations for the computations of energies and Franck-Condon factors, and thus for the computation of the time evolution of the fluorescence spectra.

There is yet another possibility which will be followed up in a subsequent study. Instead of solving the vibrational problem, we can adopt the methods developed by Heller[20] for studying wave packet dynamics. Given an inital fluid configuration—sampled by Monte Carlo—the molecular dynamics of the wave packet and fluid can be solved. This requires three classical trajectories for each initial configuration (including packet state). The beauty of this technique is that it enables us to study transitions involving highly excited states—states that are otherwise not obtainable by the perturbation techniques described above.

The procedure used to compute the Franck–Condon factors is as follows. The vibrational wave functions (for a given configuration) on surface A are

$$|\psi_n^A\rangle = \sum_k C_{nk}^A |\phi_k^A\rangle \,, \tag{2.23}$$

where $|\phi_K^A\rangle$ are harmonic oscillator states on surface A. The Franck–Condon factors are then

$$\langle\psi_n^A|\psi_m^B\rangle = \sum_{k,l} C_{n,k}^A C_{m,l}^B \langle\phi_K^A|\phi_l^B\rangle \,. \tag{2.24}$$

The coefficients are computed perturbatively as outlined in Sec. II B. The harmonic overlaps,

$$F_{kl}^{AB} \equiv \langle\phi_K^A|\phi_l^B\rangle \tag{2.25}$$

depend on the harmonic frequencies ω_A, ω_B of the two electronic surfaces, and also on the difference in the equilibrium bond lengths, $\Delta \equiv r_{e,B} - r_{e,A}$. ω_A, ω_B, and Δ and, concomittantly, the harmonic overlap, vary with fluid configuration. To avoid evaluating the overlap for every configuration, it was convenient to adopt the following procedure. First, we note that the overlaps are functions of ω_A and ω_B through the parameters γ_A, γ_B:

$$F_{kl}^{AB} \equiv F_{kl}(\gamma_A, \gamma_B\,; \Delta) \,, \tag{2.26}$$

where $\gamma_A \equiv (m\omega_A/\hbar)^{1/2}$, and $\gamma_B = (m\omega_B/\hbar)^{1/2}$ define harmonic length scales in the two surfaces. By simple change of scale of the integral defining F_{kl}^{AB}, it can be shown that

$$F_{kl}(\gamma_A, \gamma_B\,; \Delta) = (1/\gamma_A) F_{kl}(1, \gamma_B/\gamma_A, \gamma_A\Delta) \,. \tag{2.27}$$

The approach employed in the simulations was to expand $F_{kl}(1, x, y)$ in a Taylor series up to quadratic order around some average value for x_0, y_0. The matrices $F_{kl}(1, x_0, y_0)$; $(\partial F_{kl}/\partial y)(1, x_0, y_0)$; $(\partial^2 F_{kl}/\partial x^2)(1, x_0, y_0)$; $(\partial^2 F_{kl}/\partial y^2)(1, x_0, y_0)$; and $(\partial^2 F_{kl}/\partial x \partial y)(1, x_0, y_0)$ are then evaluated before the simulation is initiated. Then F_{kl} can be evaluated at each step of the simulation, from the quadratic expansion for each new x, y. The average values of x_0, y_0 are found from small trial runs. The fluctuation of x and y around x_0 and y_0 is monitored. In all cases reported, the fluctuations are sufficiently small that this Taylor series approximation should be accurate. If in other cases the fluctuations become too large, more than one such expansion point can be chosen. Then as the run proceeds for each new solvent configuration, the closest expansion point (x_i, y_i) could be seen.

III. RESULTS

A. Solvent effects on vibrational spectrum

In this section, we report the results of a number of Monte Carlo simulations of a model system consisting of Br_2 dissolved in Ar. Br_2 in Ar is a somewhat unusual system in that the vibrational period for Br_2 is about 10^{-13} s, which is quite slow as vibrational motions go. At 300 K, the temperature at which our Monte Carlo simulations are run, a free Ar atom travels about 0.3 Å per vibrational period on the average. Thus, we would expect the adiabatic approximation to break down, with the consequence that solvent induced vibrational relaxation may be rapid. The present work makes no attempt to calculate this nonadiabatic vibrational relaxation. Furthermore, it assumes that the mixed quantum-classical density matrix based upon the separation of

vibrational and rotational-translation motions provides a reasonable description for the calculation of static properties of this system. The question of solvent induced, nonresonant vibrational relaxation and the effect it has on the statistical properties of a system is a very interesting subject which we hope to address in future work.

The intramolecular Br_2 interaction is modeled by a Morse potential with $D_e = 23100$ K, $\alpha = 1.94$ Å^{-1} and $r_e = 2.28$ Å. The solvent (Ar) atoms interact with each other via a Lennard-Jones (LJ) potential with $\epsilon_{Ar} = 120$ K and $\sigma_{Ar} = 3.42$ Å. The Ar atoms interact pairwise additively with each Br atomic center through an LJ potential. In one model, designated the fixed epsilon (FE) model, the Ar–Br LJ parameters are those of Freaser *et al.*,[21] $\epsilon_{Br} = 143$ K, $\sigma_{Br} = 3.51$ Å. Since the electron density in Br_2 certainly depends on bond length, it is more realistic to use parameters in the Ar–Br potential which are dependent on r. Pratt and Chandler[5] and Oxtoby[16] have suggested that the variation of the strength of V_{Ar-Br} with changing Br_2 bond length is an important feature that must be taken into account in order to correctly reproduce the solvent effects on the oscillator. Since the molecular static polarizability is generally an increasing function of bond length, Pratt and Chandler[15] suggest replacing the constant ϵ_{Br} in B_{ArBr} with an ϵ_{Br} which is a linear function of r. (Because it is the attractive part of the LJ potential that should depend on the Br_2 polarizability, Pratt and Chandler opt for including the bond length dependence in $V^{(1)}_{ArBr}$ only. Here $V^{(1)}_{ArBr}$ is the attractive part of the total potential $V_{ArBr} = V^{(0)}_{ArBr} + V^{(1)}_{ArBr}$ as defined by Weeks, Andersen, and Chandler theory.[22] However, this leads to changes in this parameter, and give the same relength. Furthermore, there is no reason to believe that the repulsive potential $V^{(1)}_{ArBr}$ is independent of bond length. Therefore, we employ a modified bondlength dependent ϵ_{Br} for the total potential V_{ArBr}.) We adopt an $\epsilon_{Br}(r)$ which is nearly linear near r_e, but which goes to constant values at large and small r. This avoids the possibility of spurious effects due to having a potential well which increases in depth without bound as r increases. The functional form employed is[9]

$$\epsilon_{Br} = \epsilon_1 - \epsilon_2 \exp\{-\alpha'(r-b)^2\} . \tag{3.1}$$

The parameters ϵ_1, ϵ_2, α', and b are fit so that $\epsilon_{Br} = 143$ K, $(d \ln \epsilon_{Br}/dr) = 1$ Å^{-1} (this is the same slope as that used by Pratt and Chandler[15]), and $d^2\epsilon_{Br}/dr^2 = 0$ at r_e. This last condition ensures that ϵ_{Br} is approximately linear near r_e. Given these parameters, there is one free parameter in our functional form for $\epsilon_{Br}(r)$, namely, $r_e - b$. By choosing a sufficiently large value for this parameter, the region of approximately linear behavior of $\epsilon_{Br}(r)$ near r_e can be adjusted to be suitably large. In all variable epsilon (VE) studies reported below, $r_e - b = 0.5$ Å. $r_e - b = 1.0$ Å has also been tested and the results of the simulations found to be insensitive to changes in this parameter, and give the same results as $r - b = 0.5$ Å.

The Ar–Ar and the Ar–Br potentials are spherically truncated and shifted at pair distances R^c_{Ar-Ar} and R^c_{Ar-Br}, respectively. At these cutoffs, both potentials are 1 K—with the proviso that Br_2 is at its equilibrium bond length. The introduction of the cutoffs leads to discontinuities in the derivatives of the potentials at the cutoff distances, but the cutoffs are at sufficiently large distances that these discontinuities cause no problems in practice.

TABLE I. Average quantities for Br_2 in Ar model system evaluated from mixed quantum-classical Monte Carlo simulations.

		$\langle r \rangle$ (Å)	$\langle \omega \rangle$ (ps^{-1})
I.	$\chi = 0.3$, ϵ_{ArBr} is constant	2.2842	60.54
II.	$\chi = 0.3$, ϵ_{ArBr} is a function of r	2.2953	58.90
III.	$\chi = 0.6$, ϵ_{ArBr} is a function of r	2.2728	64.47
	Isolated Br_2 Morse potential	2.2861	60.152

Following Freaser *et al.*,[21] we report the density of the various simulations in terms of an effective excluded volume fraction, defined as

$$\chi = \pi(\rho_{Ar}\sigma^3_{Ar} + \rho_{Br}\sigma^3_{Br})/6 , \tag{3.2}$$

where ρ_{Ar} and ρ_{Br} are the number densities of Ar and Br atoms in the simulation, respectively.

The details of the Monte Carlo simulation procedure are the same as presented in an earlier publication[9] and are not discussed here. Runs have been performed for $\chi = 0.3$, 0.4, 0.5, and 0.6, using the variable epsilon model for the Br–Ar interaction. For comparison, a fixed epsilon run has also been performed at $\chi = 0.3$. All runs are performed at 300 K. The initial configuration for each run is taken to be the final configuration of some previous simulation, and the system is allowed to relax further for least 5.4×10^3 moves. Each run consists of 5.4×10^4 moves, in addition to the moves which are discarded at the beginning of the simulation. Some tests of the accuracy of the statistics for the simulations have been made. These are discussed below and they indicate that these simulations are sufficiently long to provide accurate results.

A number of quantities have been determined. Among these are the bond length distribution, the distribution of energies $\{\epsilon_n(\mathbf{X})\}$ in individual oscillator strates, and the distribution of harmonic frequencies of the vibrational potential defined as $\omega(\mathbf{x}) = [(1/m)(\partial^2 V(r, \mathbf{x})/\partial r^2]^{1/2}_{r_m}$. The solvent effect on the bond length is fairly small in all cases, as demonstrated by the results in Table I. Run I ($\chi = 0.3$, constant ϵ_{Br}) shows essentially no effect on the average bond length as compared with the isolated molecule. $\langle r \rangle$ increases somewhat, 0.009 Å, when the bond length dependence is added to $\epsilon_{Br}(r)$ at this density, in agreement with the prediction of Pratt and Chandler.[14] At high density ($\chi = 0.6$) with r-dependent ϵ_{Br}, there is a 0.013 Å reduction in the bond length conpared with the r for the Morse potential alone. As a check of the accuracy of these results, a second simulation $\{\chi = 0.3$, variable $\epsilon_{Br}(r)\}$ has been performed. The average bond length differed by only 0.0002 Å between these two runs, indicating that good statistics have been

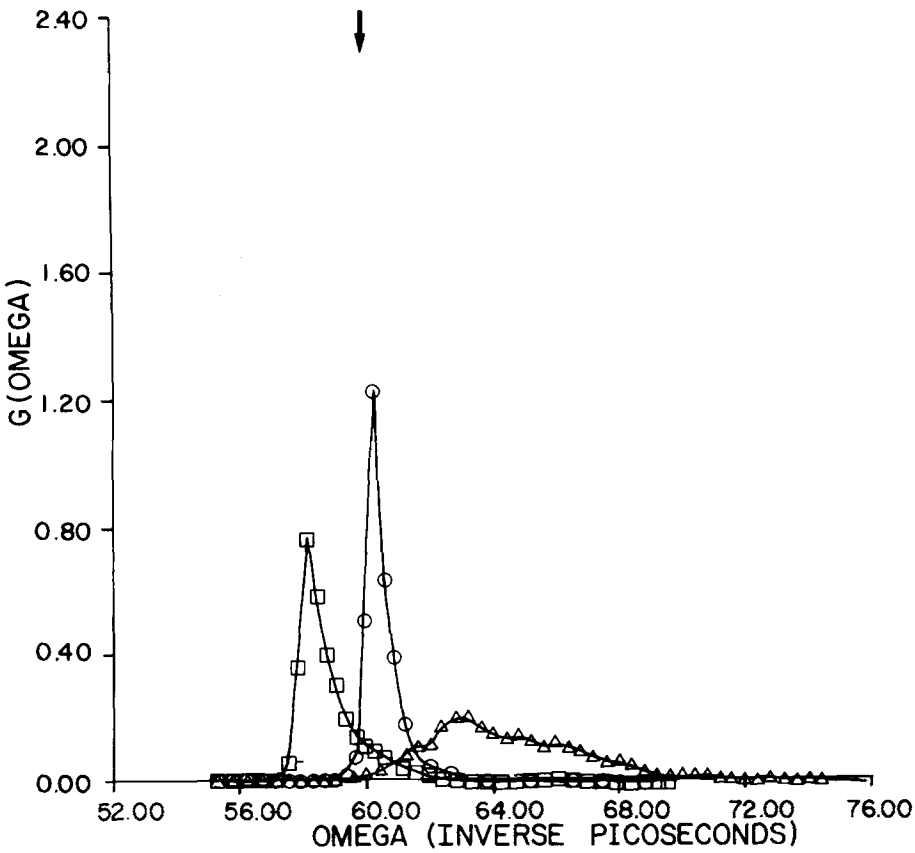

FIG. 1. Distribution of harmonic frequencies calculated from mixed quantum-classical Monte Carlo simulations. (O) $\chi = 0.3$, ϵ_{ArBr} is constant; (□) $\chi = 0.3$, ϵ_{ArBr} is a function of r, and (Δ) $\chi = 0.6$, G_{ArBr} is a function of r. The arrow marks the location of the frequency for the Morse oscillator in the absence of solvent.

achieved. (The statistics for the highest density $\chi = 0.6$ simulation appear to be poorer. For instance, if separate subaverages of the bond length are taken at this density for the first 2.7×10^4 moves and for the last 2.7×10^4 moves, these averages differ by nearly 0.01 Å. Presumably, these poor statistics are the result of decreased efficiency of sampling at the higher density due to smaller step sizes and to increased difficulty of reaching all other configurations from a given configuration because of the tight packing. Even with the poorer statistics, the qualitative trends discussed are certainly still significant.)

In contrast to the bond length, properties that are related to the internal vibrational state energies of the diatomic $\epsilon_n(X)$ are indeed sensitive to density, and also to the inclusion of the bond length dependence in $\epsilon_{Br}(r)$. The same trends are apparent whether one views the average values and distribution functions for the harmonic frequency $\omega(\mathbf{X})$, or for internal oscillator state energies, or for differences in state energies. This is not surprising, since the internal state energies are just $(n+1/2)\hbar\omega$ in lowest order. Only the data for $\omega(\mathbf{X})$ is discussed here in detail. The distribution functions of the harmonic frequencies are presented for three simulations in Fig. 1. Two of these are at $\chi = 0.3$. They differ in that in one, ϵ_{Br} is held constant, while in the other $\epsilon_{Br}(r)$ depends on bond length [Eq. (3.1)]. The third simulation also includes the variable $\epsilon_{Br}(r)$, but is at the higher density, $\chi = 0.6$. For run I ($\chi = 0.3$, fixed ϵ_{Br}), $\langle\omega\rangle = 60.54$ ps^{-1}, lies very close to the frequency for the isolated Morse potential, 60.15 ps^{-1}. Addition of the bond length dependence in $\epsilon_{Br}(r)$ gives $\langle\omega\rangle = 58.90$ ps^{-1}, and in fact induces a red shift in agreement with the qualitative prediction of Pratt and Chandler[15] and the quantitative studies of various systems by Schweitzer and Chandler.[16] The frequency distributions rise sharply on the low frequency side and tail off more slowly at high frequencies. The distribution function for the $\chi = 0.6$ simulation is much broader, blue shifted, and it does not rise as fast on the low frequency side as the $\chi = 0.3$ case. The skewing of these distributions is interesting since Gaussian approximations are sometimes employed for $g(\omega)$ [and $g(\omega, t; \omega_0, t_2)$ the two time distribution function] on the basis of a central limit argument.[23] A similar skewing has been noted by Dijkman and ver der Maas[24] in their model calculations of inhomogeneous broadening of infrared line shapes by inert solvents.

Figure 2 is a plot of the shift in the average frequency (relative to the value for the isolated Morse potential) versus density. All points correspond to simulations with bond length dependent $\epsilon_{Br}(r)$. The red shift at low frequencies which turns into a blue shift at higher frequencies is very reminiscent of similar trends seen in experimental studies on the density dependence of infrared frequencies.[14] For $\chi = 0.3$ ($\rho\sigma^3 \sim 6$) and fixed ϵ_{Br} (cf. Fig. 1), there is no shift suggesting that the red shift would be lost if the $\epsilon_{Br}(r)$ were not treated as a function of bond length as it has been in these simulations. Comparison of the results of two identical simulations at $\chi = 0.3$ suggests that the statistics of these runs are rather good. The difference in the average

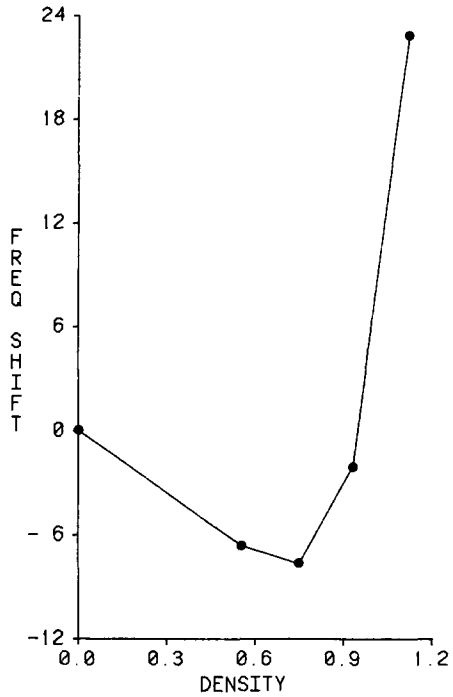

FIG. 2. $\langle\omega\rangle - \omega_0$ plotted vs density. ω_0 is the frequency of Morse potential in the absence of solvent. ω is measured in cm^{-1} and density in units of $\rho\sigma^3$ where ρ and σ are the number density and van der Waals diameter of Ar.

frequencies of the two runs is only 0.082 ps^{-1}.

As a test of the convergence of the perturbation expansion for the vibrational state energies, Table II presents results of the zeroth, second, and fourth order calculations of the internal vibrational state energies $\epsilon_n(X)$ for $n=0$ through 7 for a particular solvent configuration (taken from $\chi=0.3$) for a variable ϵ_{Br} simulation. This indicates that the fourth order perturbation calculations should provide highly accurate results.

It has been suggested that the frequency distribution should be Gaussian since the instantaneous frequency is the superposition of numerous more or less random perturbations due to the interactions of the solute with the solvent particles. To understand why this central limit argument does not predict the correct result, first consider the case of one solvent particle interacting with the diatomic. For simplicity we assume a collinear geometry. As the particles are brought closer from an infinite separation, the long range attractive solvent solute interaction causes a slight decrease of the effective harmonic frequency of the diatomic. At some separation of the diatomic and perturber the frequency goes through a minimum and for shorter separations shifts to higher frequencies as the repulsive portion of the solvent–solute interaction squeezes the vibrational coordinate. Near the minimum frequency ω_M the frequency can be expanded as a function of the solvent–solute separation variable x:

$$\omega \approx \omega_M + A(x - x_M)^2 , \tag{3.3}$$

where x_M is the value of x which corresponds to ω_M. The distribution of frequencies $g(\omega')$ is defined as the integral over all x of $\delta(\omega' - \omega)$ weighted by the Boltzmann factor

$$g(\omega') = Q^{-1} \int dx \exp\{-\beta[\tfrac{1}{2}\hbar\omega(x) + V_M(x)]\} \times \delta[\omega' - \omega(x)] , \tag{3.4}$$

where $V_M(x) \equiv V[r_M(x), x]$, $r_M(x)$ is the bond length for which $V(r, x)$ is a minimum for constant x. In Eq. (3.4) it has been assumed only that the ground vibrational state is significantly populated and that the harmonic approximation for the state energy is reasonable. Clearly for $\omega' < \omega_M$, $g(\omega') = 0$. Close to ω_M Eq. (3.3) provides the relationship between x and ω. Since

$$dx = d\omega \left(\frac{dx}{d\omega}\right) = \pm \frac{d\omega}{2[(\omega - \omega_M)/A]^{1/2}} \tag{3.5}$$

the integral over x in Eq. (3.4) can be converted into two integrals over ω [one for each branch of $\pm(\omega - \omega_M)^{1/2}$] which are easily performed yielding

$$g(\omega') = \frac{1}{[(\omega' - \omega_M)/A]^{1/2}} \exp\{-\beta[\tfrac{1}{2}\hbar\omega' + V(x(\omega))]\} \tag{3.6}$$

for ω' slightly greater than ω_M, and $x(\omega')$ is found by inverting Eq. (3.3). Therefore, the dominant behavior near ω_M is a jump from zero to ∞ at ω_M and then a subsequent decay as $[\omega - \omega_M]^{-1/2}$. Thus, the case of one perturber yields a skewed distribution.

When many solvent molecules are present, the integral over x in Eq. (3.4) is replaced by a multidimensional integral over the entire solvent configuration space. The harmonic frequency still has an absolute minimum as function of all solvent coordinates. Below this value ω_M, $g(\omega) = 0$. The δ function in the integrand of the integral over solvent configurations picks out the volume of configuration space corresponding to a given ω. Since ω_M corresponds to a single point in configuration space (actually a number of equivalent points related by interchange of solvent particles), it has zero volume and the singular behavior of the one-dimensional example does not appear. However, if the most probable frequency lies near ω_M, the low frequency wing must necessarily be truncated. This is the case at low and moderate densities since the nearest solvent particles tend to be located at distances from the diatomic at which the solvent–solute interaction is attractive. At higher densities, the repulsive portions of the inter-

TABLE II. Vibrational state energies of Br_2 in Ar from zeroth, second, and fourth order perturbation calculations for a typical configuration with $\chi = 0.3$ and ϵ_{ArBr} given by Eq. (3.1) with $r_0 - b = 0.5$ Å.

n	Zeroth order energy (K)	Second order energy (K)	Fourth order energy (K)
0	229.7	229.2	229.2
1	689.1	684.6	684.6
2	1148.5	1136.0	1136.0
3	1607.9	1583.5	1583.5
4	2067.3	2026.9	2026.6
5	2526.7	2466.3	2465.9
6	2986.1	2901.7	2901.0
7	3445.5	3333.2	3332.1

TABLE III. Morse parameters for two electronic states.

	A	B
D_e	23100 K (1.99 eV)	18000 K (1.55 eV)
α	1.94 Å^{-1}	1.86 Å^{-1}
r_e	2.28 Å	2.40 Å
$V_M(r_e)$	0	10000 K (0.862 eV) (6950.3 cm^{-1})
ω_{HO}	6.016×10^{13} s^{-1} 319 cm^{-1}	5.0912×10^{13} s^{-1} 270 cm^{-1}
ν_{HO}	9.57×10^{12} Hz	8.103×10^{12} Hz

action dominate. The most probable frequency lies far above ω_M and the low frequency cutoff is obscured since it is far out in the wings of the distribution. Therefore, $g(\omega)$ for high densities appears less skewed.

B. Solvent effects on electronic spectra

The methods outlined in Sec. II can be used to study how the solvent perturbs the electronic absorption and fluorescence spectra of diatomic molecules. In this section, we consider a fictitious diatomic molecule X_2 dissolved in various simple solvents. In its ground electronic state, labeled A, X_2 is identical to the Br_2 molecule studied in Sec. II A; however, in the excited state studied here (labeled the B state), X_2 bears no relationship to any of the excited states of Br_2. The B state intramolecular potential is also taken to be a Morse potential. The parameters used in the Morse potentials for the A and B states are given in Table III. The minimum of the B state potential is 6950.3 cm^{-1} above the minimum of the A state potential so that in the absence of solvent, and in the harmonic approximation, the $AO-BO$ transition is at 6925.9 cm^{-1}.

In Fig. 3(a) we show the exact absorption and emission spectrum for isolated X_2. This was computed using the exact states of the Morse oscillator. In Fig. 3(b) we show the spectrum determined by the perturbation treatment outlined in Sec. II B together with the numerically determined Franck–Condon factors. Comparison of Figs. 3(a) and 3(b) shows that the numerical techniques introduced here are quite good.

How does solvent perturb the electronic spectrum? This depends sensitively on the intermolecular potential between solvent and solute. It is expected that the molecule X_2 in the B state interacts differently with solvent molecules than X_2 in the A state. Because little is known about the interaction potential, we will study several simple models.

In all of the systems studied, the temperature is 85 K, and the density is $\chi = 0.4$ with one X_2 molecule and 107 solvent atoms. The potentials are spherically truncated and shifted, and periodic boundary conditions are used. Each run consists of 250 passes after initial aging. For each system separate simulations were performed with configurations sampled from the A state and from the B state. The transition energies and Franck Condon weighting factors are evaluated for the transitions from the ground vibrational state of the initial electronic state (A or B) to the first eight vibrational states of the final surface (B or A). Hot bands are thus ignored. The weighted transition energies are binned. For the case where A is the initial surface, the weighted distribution of transition energies gives the absorption spectrum, whereas when B is the initial state, a similar procedure gives the emission spectrum. In the latter case, the assumption is made that the lifetime of the B state is sufficiently long that the vibrations in that state have relaxed to the ground vibrational state, and furthermore, the solvent has fully relaxed around the B state. In two cases (the first and last below) the emission spectrum has also been computed, assuming that the solvent does not have time to relax at all.

In all of the systems studied, each X center in X_2 interacts with each solvent atom through a Lennard-Jones potential with parameters ϵ_x, σ_x which depend on whether X_2 is in the A or B state. Thus for each system we must choose $[\epsilon_x(A), \sigma_x(A)]$ and $[\epsilon_x(B), \sigma_x(B)]$ where the A and B define the state. The solvent atoms Ar interact with each other through a LJ potential with $\epsilon_{Ar} = 120$ K and $\sigma_{Ar} = 3.42$ Å as before. In one of the simulations, X_2 is treated like a heteronuclear molecule in that it is given a bond length dependent dipole molecule and the solvent atoms are given point dipole moments of magnitude 0.5 D. The dipole moment of the diatomic is modeled as a point dipole located at the center of the bond. These latter cases will be discussed shortly.

The potential parameters are defined in Table IV.

In system IV, the B state has a bond length dependent

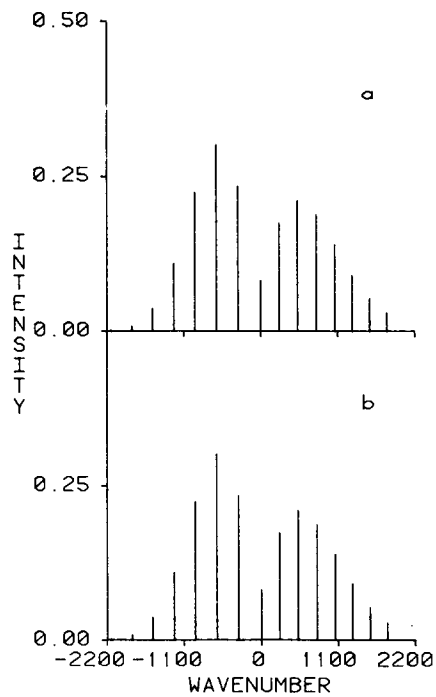

FIG. 3. Normalized intensities for vibronic absorption and emission spectra for a hypothetical diatomic in the absence of solvent. Figure 3a is evaluated by numerical integration of the exact wave functions. Figure 3b is calculated by fourth order perturbation theory. The bond length dependences of the upper and lower electronic state potential surfaces are modeled by Morse potentials. The potential parameters are given in Table III.

TABLE IV. A summary of the potential parameters used in the systems studied in this section.

System	$\epsilon_{X-X}(A)$ (K)	$\sigma_{X-X}(A)$ (Å)	$\epsilon_{X-X}(B)$ (K)	$\sigma_{X-X}(B)$ (Å)	$\mu^A_{X-X}(r_e)$ (D)	$\mu^B_{X-X}(r_e)$ (D)	Solvent μ (D)
I	143	3.51	143	3.51	0	0	0
II	143	3.51	71.5	3.51	0	0	0
III	143	3.51	143	3.69	0	0	0
IV	143	3.51	143	3.51	0	0.5	0.5

dipole moment

$$\mu(r) = 0.5\{1 + \tanh(r - 2.40)\} \tag{3.7}$$

such that at $r_e(B)$, the dipole is 0.5 D. This dipole has a linear dependence on r in the neighborhood of $r_e(B)$.

The absorption and emission spectra for these four systems are presented in Figs. 4–7. The high frequency side gives the absorption spectrum and the low frequency side gives emissions. Several comments are in order:

(i) System I has a spectrum that is very similar to the isolated molecule spectrum, except that the individual lines are inhomogeneously broadened because of solute solvent potential. The lines are slightly shifted; the shifts are smaller than the inhomogeneous line widths.

(ii) In system II $[\epsilon_{X-X}(B) = 1/2\,\epsilon_{X-X}(A)]$, the peak positions shift ~1000 cm^{-1} to the blue compared with system I $[\epsilon_{X-X}(A) = \epsilon_{X-X}(B)]$, and the peaks are much broader. This is entirely expected from the fact that in the B state, the solute solvent energy is 50% smaller than in the A state. If we assume that only the nearest neighbor solvent atoms contribute, and that there are z of these atoms, we estimate a decrease of $2z\{\epsilon_{X-X}(A) - \epsilon_{X-X}(B)\} = z\epsilon_{X-X}(A)$ in the cohesive energy of the B state relative to the A state. To account for the observed blue shift of 1440 K, all we require is on the order of ten "nearest neighbor" solvent atoms. We have somewhat more than this number, but they do not all sit at the potential minimum. In the case where $\epsilon_{X-X}(B) = 2\epsilon_{X-X}(A)$, we expect a substantial red shift in the spectrum.

(iii) In system III, $\sigma_{X-X}(B) = 1.05\sigma_{X-X}(A)$, the emission peaks shift 150 cm^{-1} to the red and the absorption peaks shift to the blue compared to system I where $\sigma_{X-X}(B) = \sigma_{X-X}(A)$. The spectral lines are much broader. The broadening clearly follows from the fact that in the B state, the molecule experiences stronger repulsions with the solvent with concommitant broadening of the individual vibrational states. Interestingly, the 00 lines for the absorptions and emissions are shifted to the blue and red, respectively. They no longer overlap. The blue shift of the absorption band can be explained by the observation that in absorption the solvent configura-

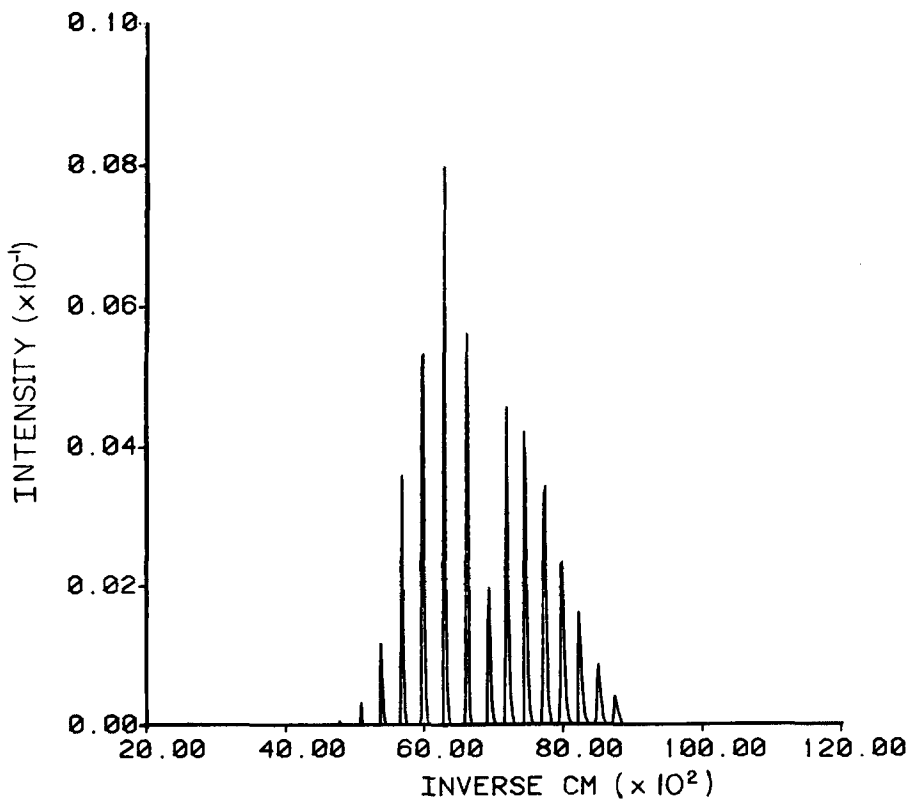

FIG. 4. Normalized vibronic absorption and emission Franck–Condon intensities for a model diatomic in a monatomic solvent system corresponding to system I of Table IV. The solvent is not allowed to relax in the evaluation of the emission spectra.

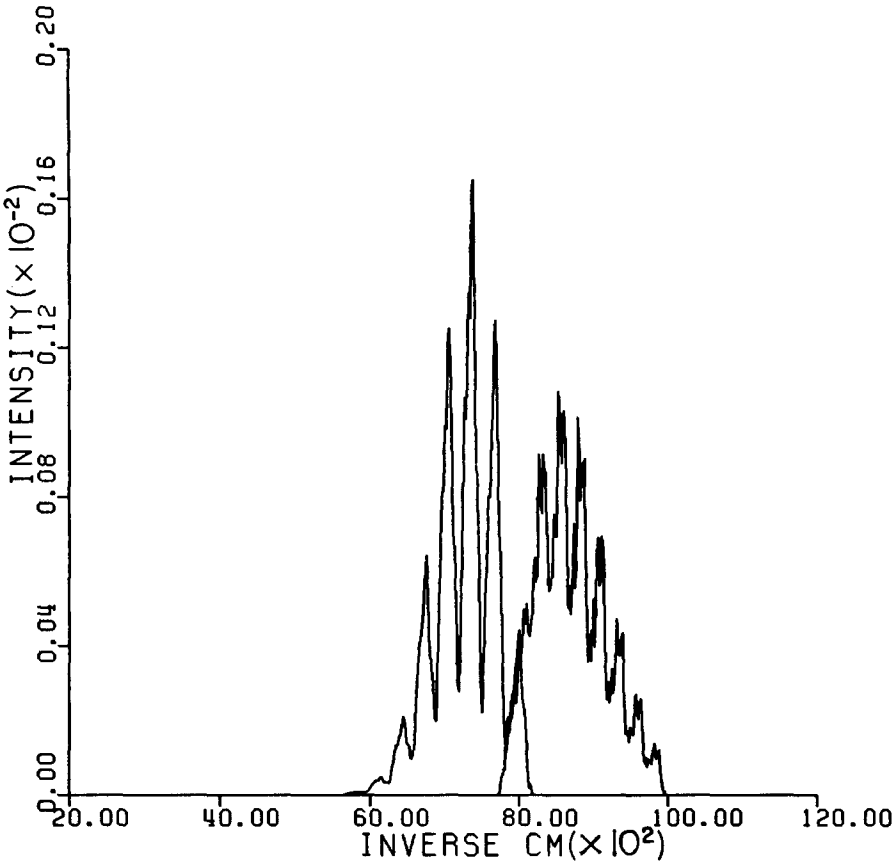

FIG. 5. Same as Fig. 4 but corresponding to system II of Table IV and the solvent is allowed to relax in the evaluation of the emission intensities.

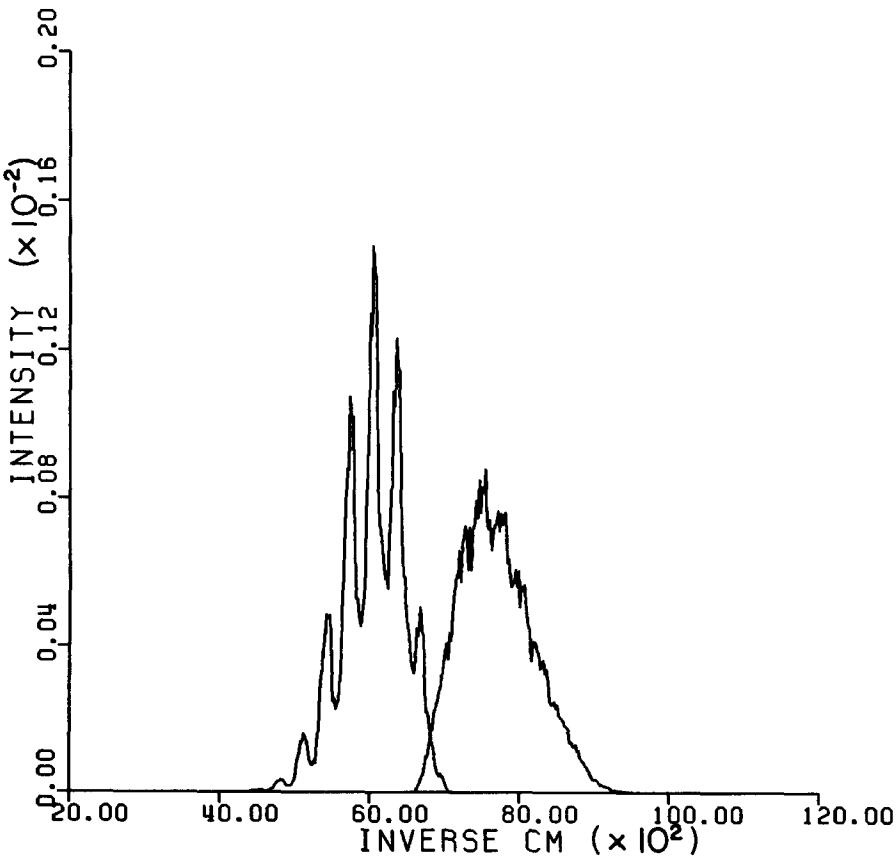

FIG. 6. Same as Fig. 4 but corresponding to system III of Table IV and the solvent is allowed to relax in the evaluation of the emission intensities.

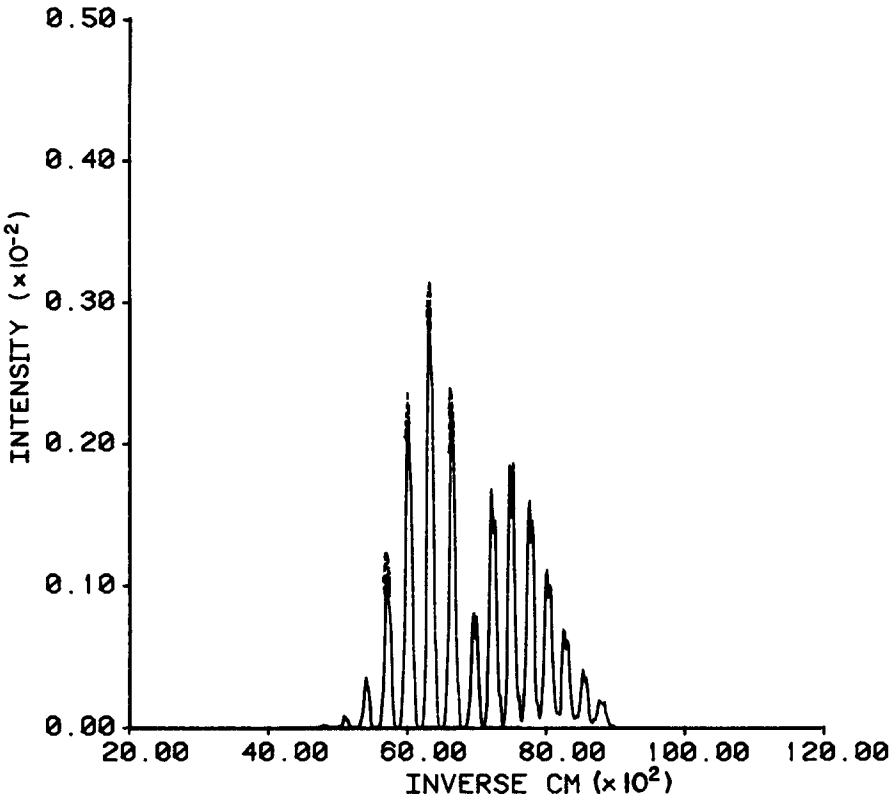

FIG. 7. Same as Fig. 4 but corresponding to system IV of Table IV. The solid line corresponds to the relaxed emission spectrum and the dotted line indicates how this changes for the unrelaxed emission spectrum.

tion is in equilibrium with the A state. For the solvent atoms near the solute, the transition to the B state is accompanied by an increase in σ_{X-X} and with a concomittant increase in potential energy. Hence, the B surface shifts up from the A surface and rises more steeply on the respulsive side. This gives a blue shift. The red shift of the emission lines can be understood as follows. The solvent is allowed to relax around the B state. Because σ_{X-X} is larger, there will now be more solvent atoms in the coordination shell with a concomittant increase in attractive energy with the B state. This lowers the energy of the A state relative to the B state.

(iv) In all cases, the absorption lines are somewhat broader than the emission lines. This is presumably because the electronically excited diatomic is slightly larger than the ground state molecule ($r_e = 2.4$ Å in the excited state versus 2.28 Å for the ground electronic state). Therefore, similar arguments to those invoked in (iii) apply. In case (III) the diatomic-solvent interaction radius σ_{X-X} is larger for the upper electronic surface than for the lower surface, causing the observed effects. However, even when $\sigma_{X-X}(B) = \sigma_{X-X}(A)$ there is still a slight effect due to the increased equilibrium bond length for the isolated diatomic for state B compared with state A.

(v) In system IV, a dipolar interaction is included; nevertheless we see very little change in the spectrum from what it was without the dipole. The spectral shifts are very small and there is only a very slight broadening. At first, this may appear surprising, but further reflection shows that at contact the dipolar interaction with one solvent is ~ 40 K. The solvent dipoles in the nearest neighbor solvent shell at 85 K will thus not be terribly ordered. Small increases in dipole moment may have profound effects on the spectra.

To better understand how the solvent perturbs the electronic absorption and emission spectra, we adopt the following simple model in which the potential curves for the A and B states are merely shifted by the solvent but are otherwise unchanged. Moreover, we assume that the potentials are harmonic. For the average frequencies of absorption we have

$$h\nu^{\text{abs}}_{0\to nB} = 1/2\,\hbar(\omega_B - \omega_A) + n_B\,\hbar\omega_B + \rho \int d^3R \int d\Omega g_A(R,\Omega)\{V_B - V_A\}\,, \quad (3.8)$$

where V_A and V_B are, respectively, the solute–solvent interaction potential in the A and B state, and $\rho g_A(\mathbf{R}, \Omega)$ is the pair correlation function giving the density of solvent molecules at a distance R from the COM of the Br_2 molecule which is oriented in space with angles Ω. The subscript A denotes the fact that the solvent is in equilibrium with the electronic state A. Similarly, g_B describes the distribution of solvent around Br_2 in equilibrium with the B state.

Likewise, the average emission frequencies are

$$h\nu^{\text{emiss}}_{0\to nA} = 1/2\,\hbar(\omega_B - \omega_A) - n_A\,\hbar\omega A + \rho \int d^3R \int d\Omega g_B(R,\Omega)\{V_B - V_A\}\,. \quad (3.9)$$

For simplicity, let us assume that the solute is a spherical molecule. From these expressions, we see that if ϵ, σ are the same in the A and B state $V_B - V_A = 0$ and there are no solvent shifts in this model. Taking $V_B(R)$

$=\epsilon_B\,\phi(R/\sigma)$, $V_A(R)=\epsilon_A\phi(R/\sigma)$ and $V_B(R)-V_A(R)=(\epsilon_B-\epsilon_A)\phi(R/\sigma)$. The integrand in Eq. (3.8) thus has the form $(\epsilon_B-\epsilon_A)\phi(R/\sigma)g_A(R)$. If $\epsilon_B-\epsilon_A>0$, this integrand has a negative well. Thus both the absorption and emission lines are red shifted from their gas phase values. Because $g_B(R)$ is more strongly peaked at the minimum than $g_A(R)$, the emission lines should be red shifted more than the absorption lines. If $\epsilon_B-\epsilon_A<0$, the integrand is positive and both the emission and absorption bands are blue shifted. Now g_A is more peaked than g_B and the absorption is blue shifted more than the emission band.

Now consider the case where $\epsilon_A=\epsilon_B$ but $\sigma_B>\sigma_A$. Then the minimum in $V_B(R)-V_A(R)$ occurs at larger distances than that for V_A. $g_A(R)$ is peaked in a region where V_B-V_A is relatively positive so that the absorption band will be shifted to the blue. $g_B(R)$ on the other hand is peaked further out in a region where V_B-V_A may be negative so that the emission band is red shifted. In all cases $\omega_A>\omega_B$ so that solvent–solute interactions destroy the resolution of the absorption line more than the emission lines. The observations are summarized below:

ϵ	σ	Emission	Absorption
$\epsilon_B>\epsilon_A$	$\sigma_A=\sigma_B$	red shift	red shift
$\epsilon_B<\epsilon_A$	$\sigma_A=\sigma_B$	blue shift	blue shift
$\epsilon_A=\epsilon_B$	$\sigma_A=\sigma_B$	no shift	no shift
$\epsilon_A=\epsilon_B$	$\sigma_B>\sigma_A$	red shift	blue shift

The simulation results are completely in agreement with this. Similar considerations lead us to believe that the dipolar system should show a significant red shift in the emission line and a much smaller red shift in the absorption lines. The dipolar energy in the solute interaction with the nearest neighbor solvent atom is ~40 °K. The solvent dipoles are randomly oriented so that there is a large cancellation of dipoles and thereby a reduction in the energy. Consequently, in the case studied, the effect of a polar solvent is rather small. We suspect that doubling of the dipole moments will lead to enormous effects. Preliminary studies using large dipole moments support this conjecture.

IV. DISCUSSION AND SUMMARY

The discussion in this manuscript has been primarily limited to systems with a single diatomic molecule in a monatomic fluid. However, many generalizations are possible. In the case of a diatomic fluid, it should be reasonable to calculate the potential of each diatomic in the field of all the other molecules fixed at their equilibrium internuclear separations. In this approximation, the vibrational problem becomes separable into individual molecular vibrations. If small polyatomics are considered, it may be feasible to solve for the normal modes of the polyatomic in the field of the solvent and use the resulting normal mode product wave function as a lowest order approximation from which perturbation corrections can be calculated. In order to study particular local features of larger solvated molecules, it might be appropriate to treat all bonds as rigid except for the few bonds in the region of interest. The torsional and possibly the bending modes could be treated classically. A better approximation for these latter types of nearly classical modes in a Monte Carlo calculation can be obtained from a discretized path integral formulation of the canonical density with a "short time" or high temperature approximation employed for the propagators involved in this formulation.[6,25,26] When these low frequency modes are nearly classical at the temperatures of interest, only a few steps would be needed in the discretized path integral for an accurate description of the quantum canonical density. Earlier we noted that the rotational motion of diatomics containing hydrogen or deuterium are known to exhibit quantum behavior in solution. This nearly classical mode could likewise be treated more accurately through a discretized path integral method.

The harmonic oscillator system serves as a very convenient zeroth order reference system. As we have shown, all the matrix elements and summations over intermediate states in the perturbation theory are independent of the solvent configuration. This greatly enhances the computational efficiency of methods of this type. We have also considered the Morse oscillator as a possible reference system. For this potential there are two energy scales, the harmonic energy scale $\hbar\omega$ associated with the curvature at r_e, and the dissociation energy D_e. In terms of appropriately scaled length and energy variables, Morse oscillators form a one parameter family of reference systems. This parameter can be chosen to be the ratio $\hbar\omega/D_e$. The Monte Carlo calculation can be set up analogously to the procedure with a harmonic reference system, except that matrix elements and the summations over states now depend on $\hbar\omega/D_e$. The approach investigated involves the initial evaluation of these quantities at a number of values of $\hbar\omega/D_e$. Interpolated values of these matrix elements and summations are obtained for the Morse oscillator that is employed as the reference potential for each configuration in the simulation. An obvious way of choosing the reference Morse potential is to pick the value of $\hbar\omega/D_e$ that reproduces the Taylor series of the solvent dependent vibrational potential through the cubic term. Our hope was that by using a better reference system, we would be able to calculate quantities relating to higher vibrational states than was possible with the harmonic potential. However, we found that the solvent induced fluctuations in the potential at large r are so great for different solvent configurations that the Morse reference potential is a poor approximation at large r. However, similar ideas may find application to other systems. For instance, the family of quartic bistable potentials (a two parameter family) may serve as an acceptable reference system for the study of a quantum bistable oscillator.

Throughout this work, model interaction potentials are chosen for the particle–particle interactions on the basis of available theoretical and experimental data. Generally, these interaction potentials are little more than intuitive models and, therefore, it is of interest to study the effect that variations in the form of the potentials have on experimentally observable quantities. The

shifting of the vibrational frequency distributions in the ground electronic state that were observed when the Lennard-Jones potential for the Br_2–Ar interaction is such that $\epsilon_{Ar-Br}(r)$ depends on the Br_2 bond length is an example of this type of investigation. The interaction between the solvent particles and electronically excited states of the diatomic is apt to be more complicated than the ground state interaction, due to the open shell nature of most excited electronic states. Moreover, less is generally known about excited molecule–solvent interactions, both theoretically and experimentally. Nevertheless (or maybe because of this), it is of interest to study the consequences of various model solvent interactions with excited electronic state molecules. We have undertaken such a study, with the various potentials outlined in Tables III and IV. This results in the various absorption and emissions spectra given in Figs. 4–7 and we easily understand these on the basis of the potential models used.

We have mentioned previously that this work rests upon the adiabatic separation of the vibrational motion from the translational and rotational motions. Nonadiabatic effects which are neglected result in solvent-induced relaxation of the vibrational populations. To test the consequences of this neglect of vibrational relaxation, the behavior of the solvent-induced nonadiabatic coupling must be studied. This coupling has the form[27] $-i\hbar\mathbf{P}_s \cdot \langle\psi|\nabla_s|\psi\rangle$ where ψ is the vibrational wave function for the system, ∇_s is the many dimensional gradient with respect to all translational and rotational coordinates, and $\mathbf{P}_s$ is the multidimensional vector composed of the conjugate momenta to these coordinates. One approach to this problem would be to run the dynamics and calculate the rate at which the first excited vibrational state is produced according to first order perturbation theory. The evaluation of the $\nabla_s\psi$ factor in the coupling would proceed very similarly to the evaluation of $\nabla_s E_n(\mathbf{R})$ described in Sec. II C, where $E_n(\mathbf{X})$ is the nth vibrational state energy.

Recently a number of workers have considered problems concerning quantum degrees of freedom in the condensed phase. One notable approach has been to study approximations to the quantum distribution function based upon the discretized representation of the path integral.[8,25,26,28,29] Applying the techniques of classical liquid state statistical mechanics to the path integral,[28,29] such quantum problems as the hard sphere model for He above the λ transition and solvation effects on a very simple model of tunneling have been analyzed. This approach may well be useful for simulating certain properties, but as matters now stand, it does not appear to offer a practical alternative to the simulations of spectra discussed here.

Wilson and co-workers[30,31] have analyzed the classical limit of infrared and Raman spectra calculated from quantum mechanical linear response theory and present quantum corrections which can be applied to rotational and vibrational spectra calculated from classical molecular dynamics. Calculations are presented for the IR spectrum of CO in Ar and the Raman spectrum of N_2 in Ar. The vibrational quantum corrections are more significant than the rotational corrections. The vibrational corrections arise from the anharmonicity of the potential and, therefore, are expected to be relatively small for such harmonic bonds N_2 and CO, as compared with the vibrations of weaker bonds. It would be interesting to test these corrections on more anharmonic systems.

To summarize, in this work we describe how the solvent induced perturbations upon vibrational modes of different electronic excited states can be studied in gases and liquids. The model is based on an adiabatic separation of vibrational and rotational/translational motions and a classical limit approximation for the latter types of motions. The key to the simulation methods discussed is the availability of a highly efficient procedure for the repeated solution of the vibrational Schrödinger equation. A perturbative method which has been found to be accurate for the low lying vibrational states is presented.

A series of Monte Carlo calculations are presented which model the Br_2 in Ar system in a high density fluid state at 300 K. In the Monte Carlo work, particular attention is paid to the distribution of harmonic frequencies for the vibrational coordinates. This distribution function is found to be a senstitive function of density. The average frequency shows a red shift at moderate densities and is blue shifted at high densities. The shift is also found to be sensitive to the form of the potential employed. In particular, the red shift is enhanced if the Ar–Br interaction is taken to be an increasing function of Br_2 bond length, in agreement with the qualitative prediction of Pratt and Chandler,[15] and the detailed studies of Schweitzer and Chandler.[16] The frequency distributions are skewed, tailing off more slowly on the high frequency side. This conclusion, which corroborates the finding of Dijkman and van der Mass,[24] raises questions about the validity of the Gaussian distribution function approximation, which is sometimes invoked on the basis of a central limit theorem argument. The skewing is less significant at higher densities.

A second electronic state on the diatomic is included in a number of simulations in order to study the distribution of vibronic transition frequencies between the ground and excited electronic levels. The well depth and interaction radius between the solvent and the electronically excited solute are varied. We find that decreasing the well depth blue shifts both the excitation (absorption) and deexcitation (emission) vibronic bands. Increasing the excited state interaction radius results in higher absorption frequencies and low emission frequencies. In each of these cases the frequency distributions are much broader than when the same solvent–solute potential is employed for the ground and excited states of the solute. This broadening is especially pronounced when the interaction radius is increased. The addition of 0.5 D dipoles to the solvent and to the electronically excited solute results in only minor changes to the vibronic frequency distributions. This indicates only partial orientational ordering of the dipoles at the temperature (85 K) considered.

[1]J. P. Valleau and S. G. Whittington, *Modern Theoretical Chemistry*, edited by B. J. Berne (Plenum, New York, 1977), Vol. 5; J. P. Valleau and G. M. Torrie, *ibid.*
[2]F. H. Stillinger, Adv. Chem. Phys. **31**, 1 (1975).
[3]R. M. Stratt and W. H. Miller, J. Chem. Phys. 67, 5894 (1978).
[4]J. D. Doll and L. E. Meyers, J. Chem. Phys. **71**, 2880 (1979).
[5]D. Ceperley and M. H. Kalos, *Monte Carlo Methods in Statistical Physics*, edited by K. Binder (Springer, Berlin, 1979).
[6]P. A. Whitlock and M. H. Kalos, J. Comput. Phys. **30**, 351 (1979).
[7]D. M. Ceperly and B. J. Alder, Phys. Rev. Lett. **45**, 566 (1980).
[8]J. A. Barker, J. Chem. Phys. **70**, 2914 (1979).
[9]M. F. Herman and B. J. Berne, Chem. Phys. Lett. **77**, 163 (1981).
[10]H. Okabe, *Photochemistry of Small Molecules* (Wiley, New York, 1978).
[11]G. Baym, *Lectures in Quantum Mechanics* (Benjamin, New York, 1969).
[12]R. P. Feynman, *Statistical Mechanics* (Benjamin, Reading, Mass., 1972).
[13]N. Metropolis, A. W. Metropolis, M. N. Rosenbluth, A. H. Teller, and E. Teller, J. Chem. Phys. **21**, 1087 (1953).
[14]W. Schindler and J. Jonas, J. Chem. Phys. **72**, 5019 (1980), for example.
[15]L. R. Pratt and D. Chandler, J. Chem. Phys. **72**, 4045 (1980). This was based on a suggestion made by D. W. Oxtoby.
[16]K. F. Schweizer and D. Chandler, J. Chem. Phys. **76**, 2296 (1982).
[17]H. Goldstein, *Classical Mechanics* (Addison–Wesley, Reading, Mass., 1950).
[18]P. Morse, Phys. Rev. **34**, 57 (1929).
[19]L. L. Sprandel and C. W. Kern, Mol. Phys. **24**, 1383 (1972).
[20]E. J. Heller, Acc. Chem. Phys. **14**, 268 (1981).
[21]B. C. Freasier, D. L. Jolly, N. D. Hamer, and S. Nordholm, Chem. Phys. **38**, 293 (1979).
[22]H. C. Andersen, D. Chandler, and J. D. Weeks, Adv. Chem. Phys. **34**, 105 (1976).
[23]R. Kubo, in *Fluctuations, Relaxation and Resonance in Magnetic Systems*, edited by D. ter Haar (Oliver and Boyd, Edinburgh, 1962).
[24]F. G. Dijkman and J. H. van der Maas, J. Chem. Phys. **66**, 3871 (1977).
[25]M. F. Herman, E. J. Bruskin, and B. J. Berne, J. Chem. Phys. **76**, 5150 (1982); R. Hall, M. Herman, and B. J. Berne (in preparation).
[26]T. Morita, J. Phys. Soc. Jpn. **35**, 980 (1973).
[27]E. E. Nikitin, *Theory of Elementary Atomic and Molecular Processes in Gases* (Clarendon, Oxford, 1974).
[28]D. Chandler and P. G. Wolynes, J. Chem. Phys. **74**, 4078 (1981).
[29]K. S. Schweizer, R. M. Stratt, D. Chandler, and P. G. Wolynes, J. Chem. Phys. **75**, 1347 (1981).
[30]P. H. Berens and K. R. Wilson, J. Chem. Phys. **74**, 4872 (1981).
[31]P. H. Berens, S. R. White, and K. R. Wilson, J. Chem. Phys. **75**, 515 (1981).